Kovove Mater. 59 2021 217–229
DOI: 10.4149/km_2021_4_217

Electromagnetic welding of Al-Cu: An investigation on the thickness of sheets

M. Ayaz[1], M. Khandaei*, Y. Vahidshad[2]

[1] *Faculty of Materials and Manufacturing Processes, Malek-Ashtar University of Technology, Tehran, Iran*
[2] *Space Transportation Research Institute, Iranian Space Research Center, Tehran, Iran*

Received 9 January 2021, received in revised form 4 April 2021, accepted 18 August 2021

Abstract

The selection of the desired thickness of sheets is of significant importance in electromagnetic welding (EMW) in order to improve the mechanical properties of joints. For this purpose, the influence of the thickness of Al, Cu, and driver sheets on the ultimate tensile strength, elongation, weld width, and hardness of the Al-Cu joint was investigated. The finite element analysis combined with the weldability window was applied to predict the joint formation. The experiments were conducted using the response surface methodology (RSM) to estimate the optimal values of sheet thickness. Then, the microstructure of the weld interface was observed by optical and scanning electron microscopy to evaluate the quality of welds. It was observed that the values of ultimate tensile strength, elongation, weld width, and hardness could be simultaneously improved by selecting the desirable values of the sheet thickness. Morphological analysis of Al-Cu weld exhibited that different impact velocities changed the shape and structure of the interface.

K e y w o r d s: electromagnetic welding (EMW), tensile properties, weld interface, response surface methodology (RSM), sheet thickness

1. Introduction

The welding of dissimilar materials of aluminum (Al) and copper (Cu) is widely used for different applications such as tube sheets, capacitors, heat-exchanger tubes, and electrical connectors. One of the issues of metallurgical reactions is the formation of intermetallic phases in the welds [1]. The brittle nature of the intermetallic phases makes them susceptible to the formation of various welding defects and thus diminishes the strength of welds [2]. Electromagnetic welding (EMW) is one of the best methods for welding the Al and Cu sheets because this process is a rapid, spotless, reliable, and cost-effective. In the EMW process, the heat input caused by the deformation of the parts is not sufficient to form thick intermetallic phases. In this process, the joint formation between the sheets is complicated, and it can be achieved within the limited range of parameters due to difficult control of the magnetic field for sheet metals [3, 4]. Thus, optimizing the significant parameters is an essential step in the EMW process for achieving a high-quality weld with a minimum thickness of the intermetallic phase. The EMW of Al-Cu sheets has been performed by several groups of researchers [2–8]. Despite the admirable attempts of earlier researchers in investigating the EMW of Al-Cu sheets, the effect of sheet thickness as effective parameter was not seen in the previous researches. A proper combination of sheet thickness configurations should be selected to ensure joint formation between the sheets. When the thickness of the sheet is too low, the leakage of magnetic flux through the sheets increases, resulting in a reduction in the impact velocity, leading to no joint formation. Also, when the thickness of the sheet is too high, the stiffness of the sheets increases, resulting in a reduction in the impact velocity, leading to no joint formation. In addition, the simultaneous investigation of the EMW parameters for developing a regression model has not been documented so far. Therefore, in this study, it was decided to use the response surface methodology to develop an experimen-

*Corresponding author: tel.: +989123963682; fax: +982122945141; e-mail address: m_khandaei@mut.ac.ir

Table 1. Mechanical properties of Aluminum 1050 and pure copper [3, 4]

Materials	A (MPa)	B (MPa)	C	n	Density (kg m^{-3})	Young's modulus (GPa)	Poisson's ratio	Hardness Hv
Al	140	75.2	0.0125	0.65	2700	69	0.33	43
Cu	90	292	0.025	0.31	8960	124	0.34	51

tal model for optimizing the mechanical properties of welds.

2. Simulation of EMW process

Finite element (FE) simulations of the EMW process are of significant interest for researchers. However, it is complicated due to the coupled mechanical, thermal, and electromagnetic aspects. By introducing the EM module, developed in LS-Dyna software, all three aspects of the EMW process can be coupled [3]. In the process simulation, the copper coil is considered a rigid body, and the Al and Cu sheets are considered deformable bodies. The values of standoff distance between the sheets and discharge voltage were kept constant at 1.5 mm and 11 kV, respectively. The Al driver sheet was applied behind the Cu sheet to accelerate its movement. The dimensions of Al and driver sheets were $60 \times 50 \times (0.5, 0.75, 1)$ mm^3, and the dimensions of the Cu sheet were $60 \times 40 \times (0.3, 0.4, 0.5)$ mm^3. The current pulses were recorded by a Rogowski coil during the EMW process by conducting some preliminary experiments. These primary current pulses were applied as the input loads for the simulation of the process. The magnetic and electrical properties of Al and Cu sheets were then utilized as inputs in the software. The constitutive model applied for the workpieces was a Johnson-Cook model, as given by the following Eq. (1):

$$\sigma = (A+B\varepsilon^n)\left(1+CLn\left(\frac{\dot{\varepsilon}}{\dot{\varepsilon}_0}\right)\right)\left(1-\left(\frac{T-T_\mathrm{r}}{T_\mathrm{m}-T_\mathrm{r}}\right)^m\right), \tag{1}$$

in which the parameters A, B, C, m, and n are material properties, $\dot{\varepsilon}$ is strain rate, $\dot{\varepsilon}_0$ is reference strain rate, T_r is room temperature, and T_m is melting temperature. The material properties and constants of Johnson-Cook are listed in Table 1. To determine the impact velocity and angle accurately, several nodes were chosen at the same positions on Al and Cu sheets. The measured values of impact velocity and angle were compared with the weldability window of Al-Cu sheets to predict the weld formation.

The weldability windows of metals have been constructed to determine the optimum parameters of impact welding [10]. The main parameters of impact welding, such as impact velocity (V_i), impact point velocity (V_c), and impact angle (β), are shown in Fig. 1.

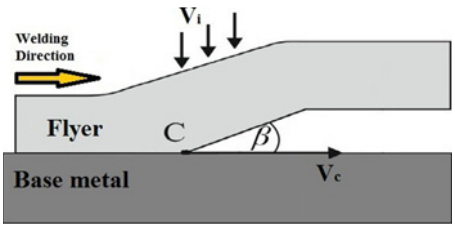

Fig. 1. Parameters of impact welding.

Table 2. Design matrix of parameters based on RSM

Parameter	Levels		
t_Al (mm)	0.5	0.75	1
t_Cu (mm)	0.3	0.4	0.5
t_Dr (mm)	0.5	0.75	1

These parameters are related together by the following Eq. (2):

$$\tan\beta = \frac{V_\mathrm{i}}{V_\mathrm{c}}. \tag{1}$$

The weldability window is developed for explosive welding, in which the impact angle (β) versus the impact point velocity (V_c) is plotted. The weldability window had also been applied for the EMW process by some researchers [4, 11]. In this study, the weldability window of Al-Cu was constructed using the proposed experimental relations in [10].

3. Experimental procedure

The EMW process was conducted according to the response surface methodology to model the effects of thickness parameters such as thickness of Al (t_Al), thickness of Cu (t_Cu), and thickness of driver (t_Dr) on the responses of the ultimate tensile strength (UTS), elongation (El), weld width (Ww), and hardness (Hv). Response surface methodology (RSM) combines mathematical and statistical techniques that are beneficial for modeling and analyzing the multi parameters problems [12]. The statistical software Minitab® 17 was used to design the experiments and analyze the obtained data. Each of the thickness parameters was considered at three levels, as given in Table 2. The different levels of the parameters are se-

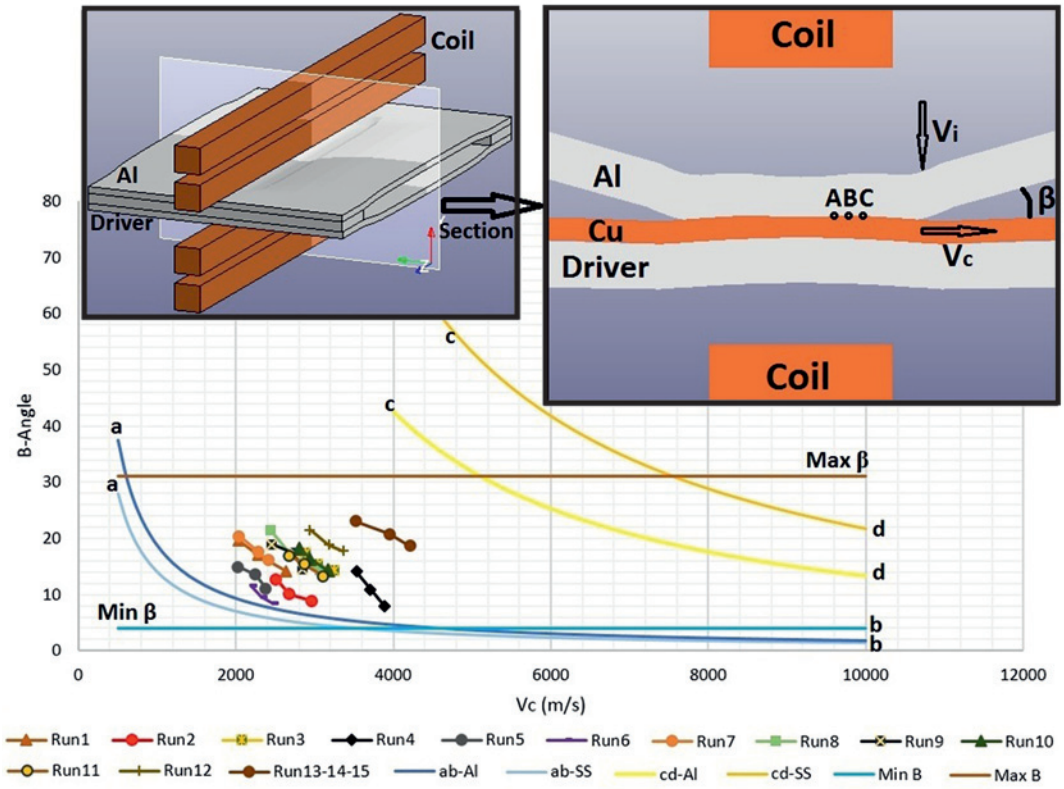

Fig. 2. Results of 15 runs of simulation in weldability window of Al-Cu weld.

lected in such a way as to achieve a good joint between the sheets. According to the response surface design, 15 experiments, including three center points, were considered to measure the responses for each experiment.

The electromagnetic welding setup consists of a power supply, capacitor bank, coil, spark gap, and workpieces. During the process, a transient magnetic field is generated around the coil, which induces eddy currents with opposite direction in the workpieces, and therefore, a repulsive force produces between the coil and the workpieces. This force can drive the workpieces together very fast, leading to a metallurgical joint formation [4]. Diffusion of the induced eddy currents into the workpieces depends upon the skin depth. The skin depth (δ) is given by Eq. (3):

$$\delta = \frac{1}{\sqrt{\pi\sigma\mu f}}, \tag{3}$$

where σ is the conductivity of the workpiece (m Ω^{-1}), μ is the permeability of the workpiece (H m^{-1}), and f is the frequency of transient current (Hz). If the skin depth is one-third of the sheet thickness or less, the magnetic field does not leak from the workpiece [5]. For welding of Al to Cu sheets, an I-shape flat two-layer copper coil was constructed. The two-layer coil reduces the discharge energy of welding. The capacitor bank used in this study was 60 μF, consisting of two parallel capacitors of 30 μF. By conducting the EMW process at the voltage of 11 kV, the first current peak was obtained to be 120 kA.

According to the ASTM-E8 standard, the samples were prepared for finding the ultimate tensile strength and elongation. The tensile samples were failed outside the weld region, showing that the weld was stronger than the weaker base metal. The cross-section of the weld specimens was then analyzed by metallographic examinations to measure the weld width and hardness of Al-Cu joints. Optical microscope (OM) and scanning electron microscope (SEM) equipped with an energy dispersive X-ray (EDX) analyzer were also used to evaluate the weld interface of Al-Cu welded sheets.

4. Results and discussion

4.1. Simulation results

The numerical simulation of the EMW process was carried out within the range of the thickness parameters to predict the probability of joint formation between the sheets. For this purpose, several nodes along the weld width were chosen to determine the impact velocity and angle of the sheets. Figure 2 shows the position of selected nodes on the cross-section of de-

Table 3. The Box-Behnken experimental design results

Run	1	2	3	4	5	6	7	8	9	10	11	12	13	14	15
t_{Al} (mm)	0.5	1	0.5	1	0.5	1	0.5	1	0.75	0.75	0.75	0.75	0.75	0.75	0.75
t_{Cu} (mm)	0.3	0.3	0.5	0.5	0.4	0.4	0.4	0.4	0.3	0.5	0.3	0.5	0.4	0.4	0.4
t_{Dr} (mm)	0.75	0.75	0.75	0.75	0.5	0.5	1	1	0.5	0.5	1	1	0.75	0.75	0.75
UTS (MPa)	70.6	71.16	72.81	73.05	68.56	69.04	69.17	70.25	69.84	70.98	70.33	71.87	73.91	74.22	74.13
El (%)	14.2	14.6	12.4	14.1	14.4	15.3	12.6	13.2	14.7	14.2	14.5	12.2	11.5	12.0	11.6
Ww (μm)	843	865	892	1041	820	846	901	938	955	1059	972	1130	1182	1197	1210
Hv (0.1 kgf)	48.3	50.8	50.4	52.5	47.6	50.1	49.4	50.5	50.1	51.2	51.5	52.0	52.9	53.1	53.4

formed sheets. In addition, the weldability window of Al-Cu is shown in Fig. 2.

In the weldability window, line "ab" represents the minimum angle of β, which is necessary for jet formation, line "ef" represents the lower limit of impact pressure which is necessary for jet formation, and line "cd" represents the upper limit of impact pressure above which interfacial melting will occur. The lower and upper limits of the dynamic angle β were experimentally suggested to be 2°–3° and 31°, respectively [10]. It should be noted that two lines were drawn for each of the Al and Cu sheets. From the simulation results, the impact velocity (V_i) and impact angle (β) of the sheets are recorded, and then the impact point velocity (V_c) is calculated by Eq. (2). If the obtained values of impact point velocity (V_c) and impact angle (β) were placed inside the weldability window of Al-Cu, a metallic bond could be formed. According to Fig. 2, all designed experiments have been located inside the weldability window, and therefore a metallic bond can be formed between Al and Cu sheets within the selected range of parameters. To verify the results of simulations, the EMW process was performed corresponding to Table 3. It was found that the weld was formed between Al and Cu sheets under different conditions of experimental design, as expected from the simulation results.

4.2. Experimental results

The average of experimental results with two replicates is listed in Table 3. The measured values of UTS, El, Ww, and Hv were evaluated using the analysis of variance (ANOVA) to find the significant parameters [12]. It should be noted that the tensile test results represent the UTS of Al base metal and not the shear strength of the weld since all the welded samples were broken from the Al base metal. After discarding the insignificant parameters from the results of ANOVA, four quadratic regression models were developed for each response. The regression models for UTS, El, Ww, and Hv were estimated as follows, Eqs. (4)–(7):

$$\mathrm{UTS} = 74.08 + 0.29t_{Al} + 0.84t_{Cu} + 0.40t_{Dr} - 1.84t_{Al} \times t_{Al} - 2.99t_{Dr} \times t_{Dr}, \quad (4)$$

$$\mathrm{El} = 11.7 + 0.45t_{Al} - 0.64t_{Cu} - 0.76t_{Dr} + 1.05t_{Al} \times t_{Al} + 1.07t_{Cu} \times t_{Cu} + 1.1t_{Dr} \times t_{Dr} - 0.45t_{Cu} \times t_{Dr}, \quad (5)$$

$$\mathrm{Ww} = 1196 + 29.2t_{Al} + 60.8t_{Cu} + 32.6t_{Dr} - 219t_{Al} \times t_{Al} - 66t_{Cu} \times t_{Cu} - 100t_{Dr} \times t_{Dr} + 32t_{Al} \times t_{Cu}, \quad (6)$$

$$\mathrm{Hv} = 53.13 + 1.03t_{Al} + 0.67t_{Cu} + 0.55t_{Dr} - 2.22t_{Al} \times t_{Al} - 1.52t_{Dr} \times t_{Dr}, \quad (7)$$

These equations were used to draw the main effects of t_{Al}, t_{Cu}, and t_{Dr} on the responses, as shown in Fig. 3. It can be seen from Fig. 3 that an increase in t_{Al} from 0.5 to 0.75 mm led to an improvement in the values of UTS by 2.7 % (Fig. 3a), Ww by 27.4 % (Fig. 3c), and Hv by 6.3 % (Fig. 3d), while it deteriorated the value of El by 4.6 % (Fig. 3b). Moreover, an increase in t_{Al} from 0.75 to 1 mm resulted in the reduction of about 1.85 % in UTS (Fig. 3a), 19.3 % in Ww (Fig. 3c), and 2.1 % in Hv (Fig. 3d), but it improved the value of El by 11.7 % (Fig. 3b). The improvement of UTS, Ww, and Hv by increasing the value of t_{Al} from 0.5 to 0.75 mm can be explained in terms of the skin depth of the Al sheet. As the value of t_{Al} raised, a considerable value of magnetic fields was confined within the thickness of sheets, and leakage of the magnetic flux through the sheets was decreased to a minimum value [5]. This occurrence provoked an enhancement in the impact velocity of the sheets and consequently led to an increase in the values of UTS, Ww, and Hv. However, a rise in the value of t_{Al} from 0.75 to 1 mm elevated the weight and stiffness of the Al sheet, which was accompanied by the higher resistance of the Al sheet against internal deformation and thus a decrease in the impact velocity of the sheets. The decrease in the impact velocity of the sheets was associated with a reduction in the values of UTS, Ww, and Hv. It should be noted that an increase in the impact velocity of the sheets led to an enhancement in the strain hardening rate of the Al sheet, which resulted in an improvement in the value of UTS and, conversely, a reduction in the value of El.

From Fig. 3, it can also be seen that the rise in t_{Cu} from 0.3 to 0.5 mm constantly enhanced the values of UTS (Fig. 3a), Ww (Fig. 3c), and Hv (Fig. 3d) by 2.4, 13.4, and 2.7 %, respectively. In addition, a rise

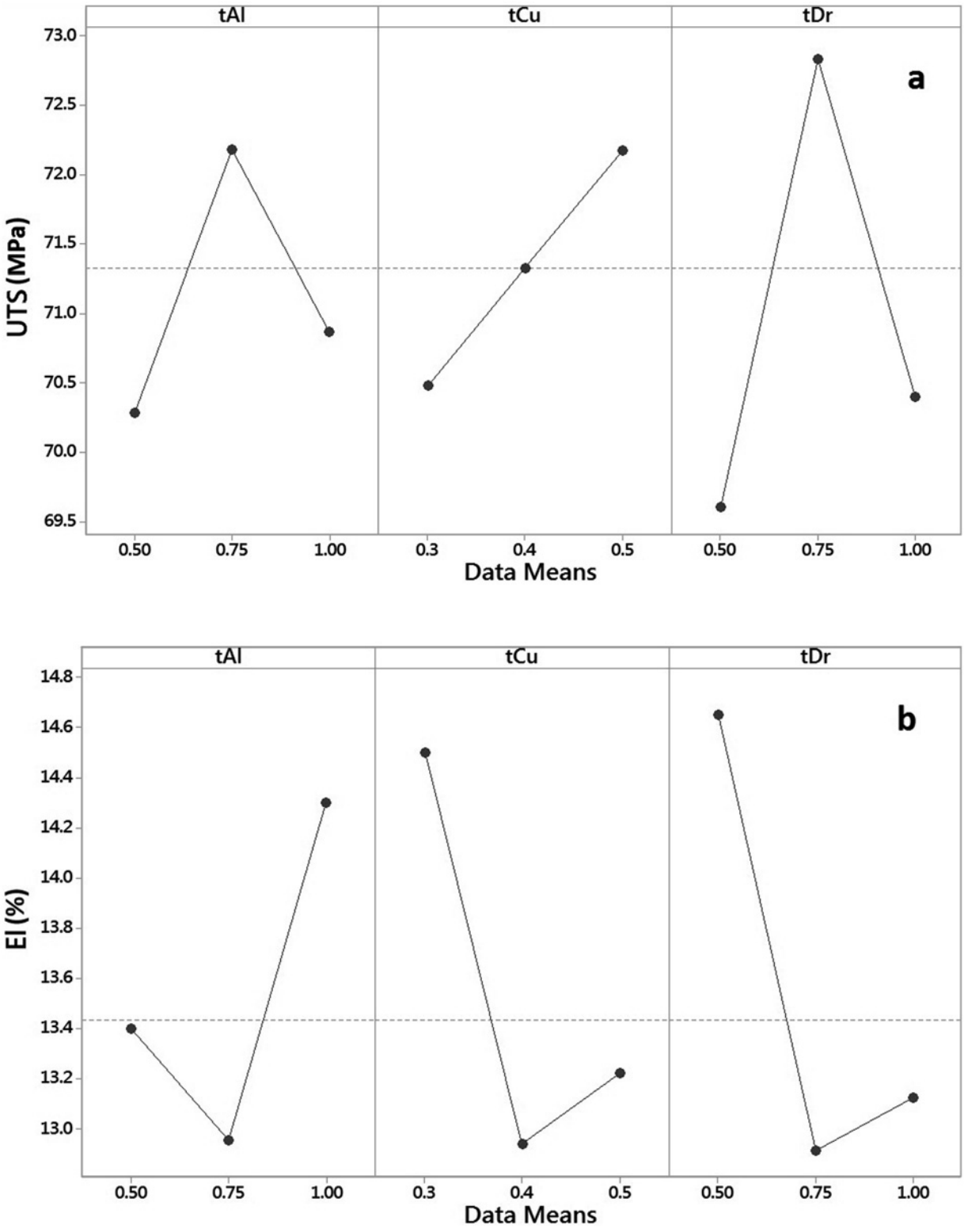

Fig. 3ab. Main effect plot of t_{Al}, t_{Cu}, and t_{Dr} on (a) UTS, (b) El.

in t_{Cu} from 0.3 to 0.5 mm firstly reduced the value of El by 13.3 % and eventually improved it by 3.9 % (Fig. 3b). It can be explained that an increase in the value of t_{Cu} was accompanied by a rise in the shielding of the magnetic fields, which resulted in the higher velocity of the Cu sheet before the collision and conse-

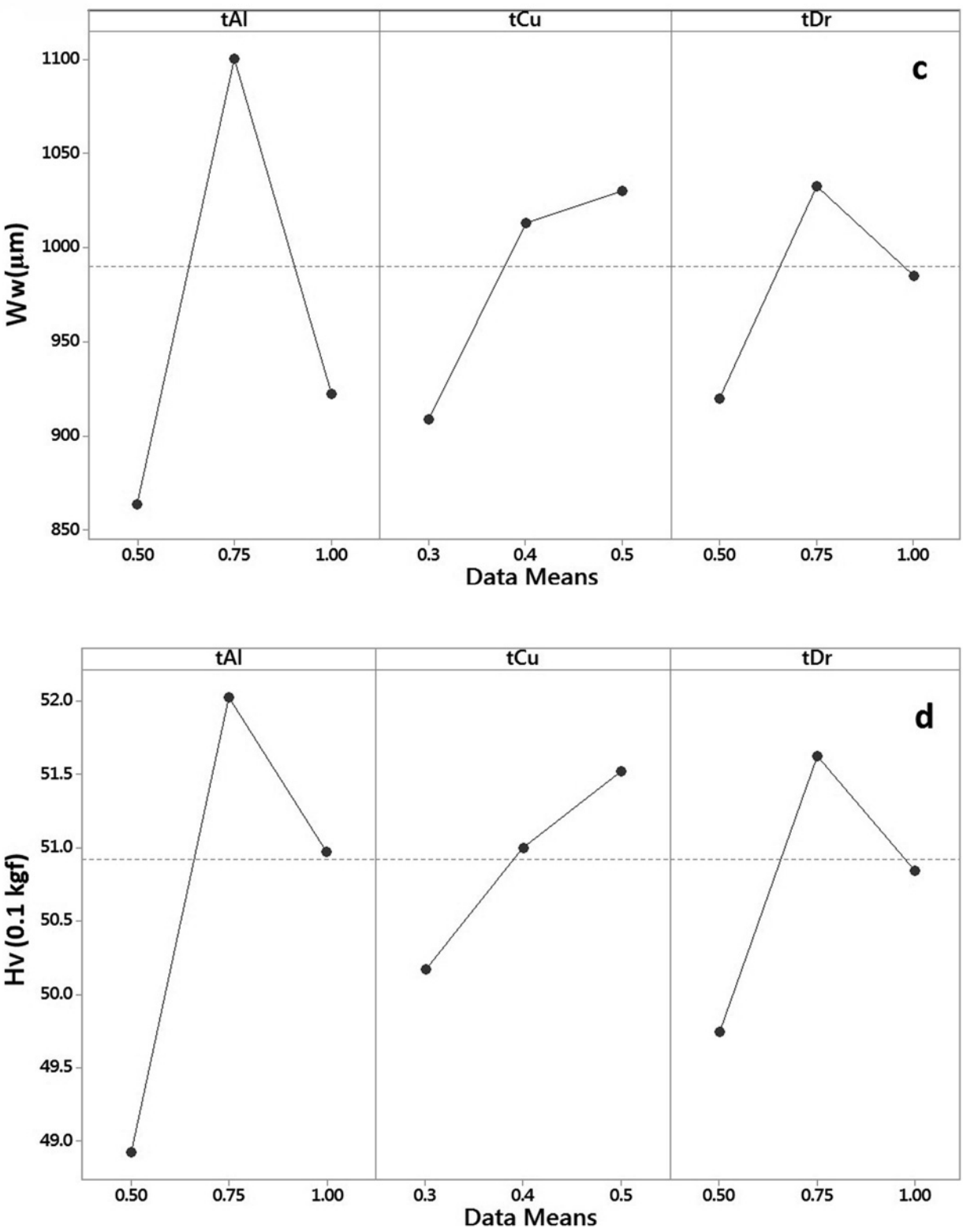

Fig. 3cd. Main effect plot of t_{Al}, t_{Cu}, and t_{Dr} on (c) Ww, and (d) Hv.

quently led to an increase in the values of UTS, Ww, and Hv and a decrease in the value of El. Moreover, it is obvious from Fig. 3 that an increase in t_{Dr} from 0.5 to 0.75 mm followed by an enhancement of about 4.6 % in UTS (Fig. 3a), 12.3 % in Ww (Fig. 3c), and 3.7 % in Hv (Fig. 3d), while an increase in t_{Dr} from

0.75 to 1 mm resulted in a reduction of about 3.4 % in UTS (Fig. 3a), 4.8 % in Ww (Fig. 3c), and 1.5 % in Hv (Fig. 3d). The value of El was also reduced by 31.5 % as the value of t_{Dr} increased from 0.5 to 0.75 mm, but it increased by 3.1 % as the value of t_{Dr} increased from 0.75 to 1 mm (Fig. 3b). The main reason for these variations can be explained in terms of the variations of the impact velocity. When the value of t_{Dr} increased up to 0.75 mm, the leakage of magnetic fields from the driver sheet was reduced. Therefore, the driver sheet increased the velocity of the Cu sheet and consequently enhanced the values of UTS, Ww, and Hv. However, an increase in the value of t_{Dr} up to 1 mm improved the stiffness of the driver sheet and so resulted in a decrease in the velocity of the Cu sheet. The decrease in the velocity of the Cu sheet reduced the values of UTS, Ww, and Hv and improved the value of El.

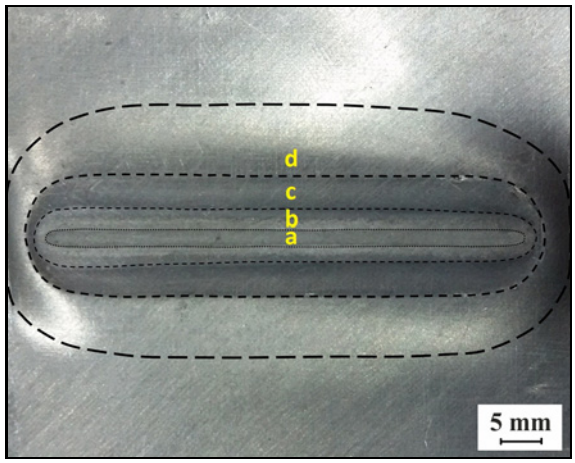

Fig. 4. Different zones in Al sheet: (a) non-welded zone, (b) weld zone, (c) collision zone, and (d) plastic deformation zone.

4.3. Characterization of the microstructure and morphology of Al-Cu weld

In this section, the effect of sheet thickness on the response was investigated by analyzing the microstructure and morphology of Al-Cu welded sheets. The welded Al sheet can be divided into four zones,

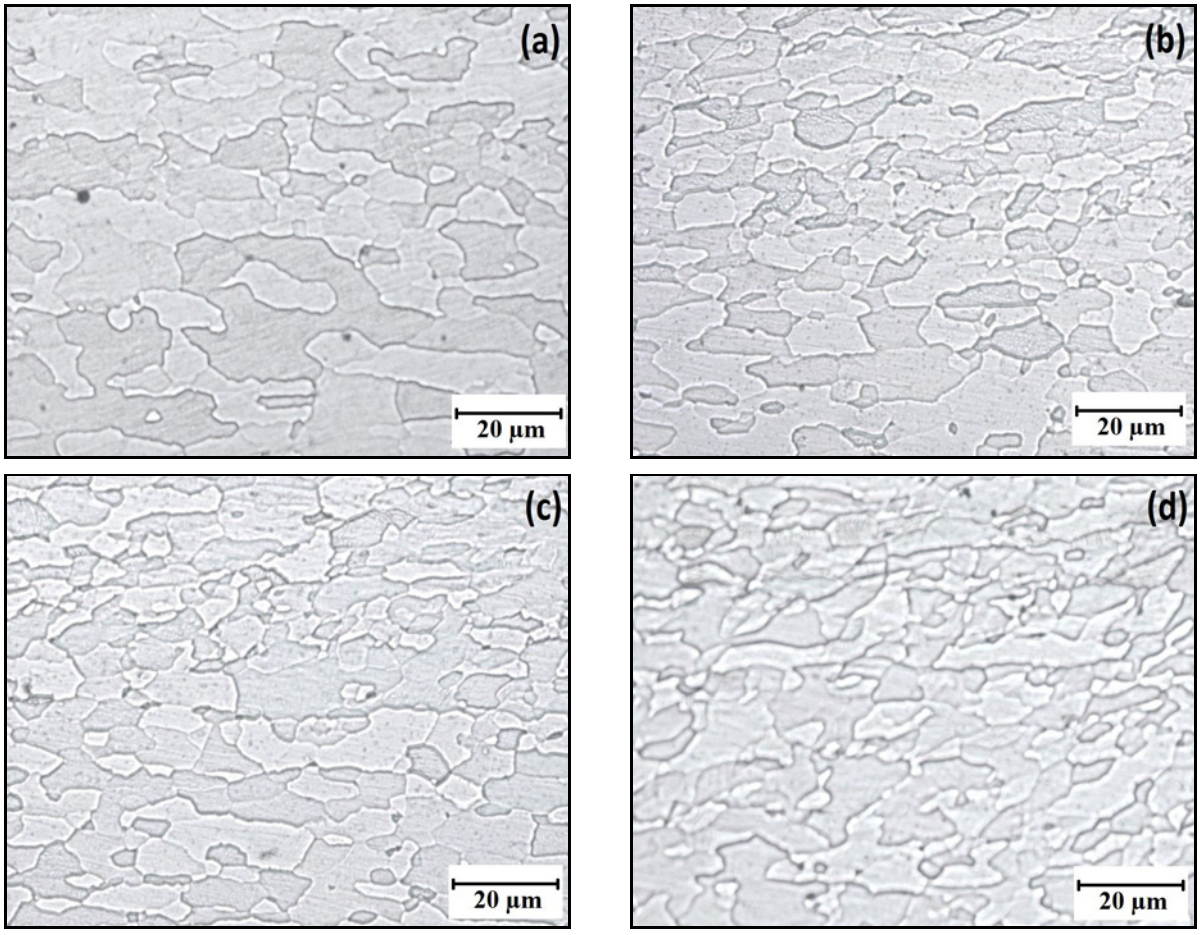

Fig. 5. Microstructure evolution of Al sheet observed at parameters of: (a) $t_{Al} = 0.5$, $t_{Cu} = 0.3$, $t_{Dr} = 0.5$; (b) $t_{Al} = 0.75$, $t_{Cu} = 0.3$, $t_{Dr} = 0.5$; (c) $t_{Al} = 0.5$, $t_{Cu} = 0.4$, $t_{Dr} = 0.5$; (d) $t_{Al} = 0.5$, $t_{Cu} = 0.3$, $t_{Dr} = 0.75$.

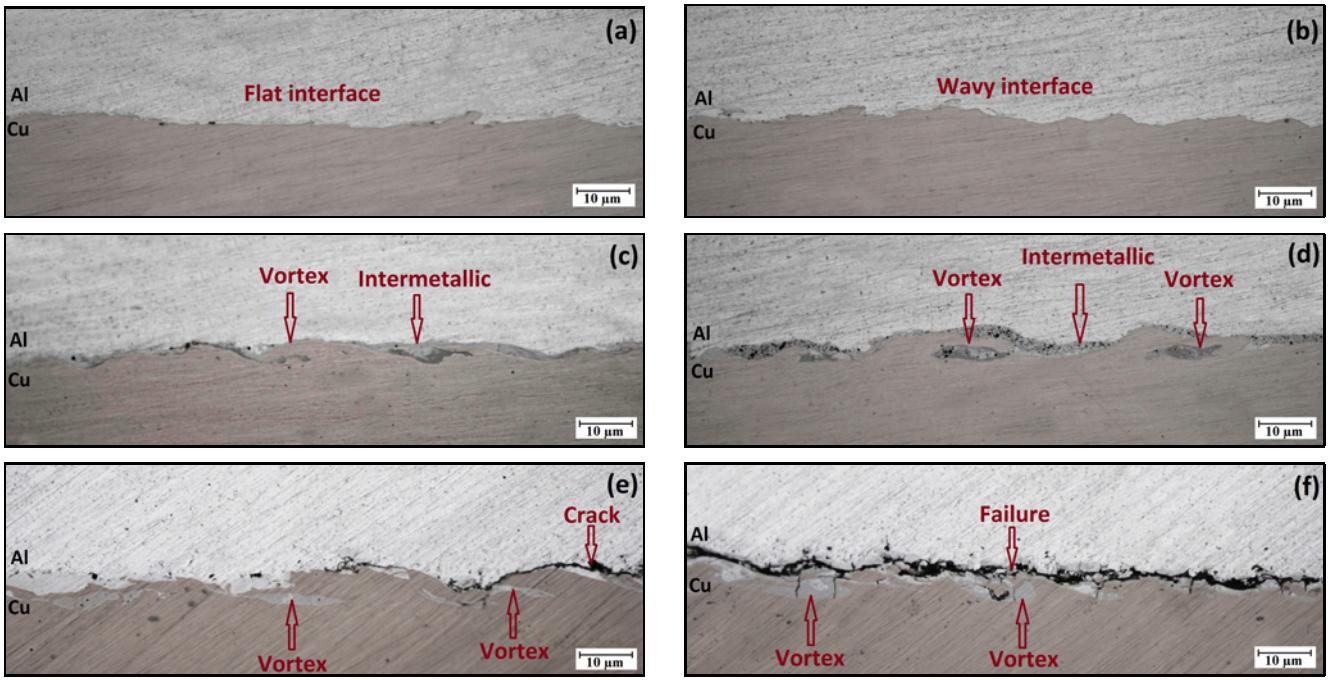

Fig. 6. Morphology of Al-Cu interface observed at parameters of: (a) $t_{Al} = 0.5$, $t_{Cu} = 0.3$, $t_{Dr} = 0.5$; (b) $t_{Al} = 0.75$, $t_{Cu} = 0.3$, $t_{Dr} = 0.5$; (c) $t_{Al} = 0.5$, $t_{Cu} = 0.3$, $t_{Dr} = 0.75$; (d) $t_{Al} = 0.75$, $t_{Cu} = 0.4$, $t_{Dr} = 0.75$; (e) $t_{Al} = 0.75$, $t_{Cu} = 0.4$, $t_{Dr} = 0.75$, V = 12 kV; (f) $t_{Al} = 0.75$, $t_{Cu} = 0.4$, $t_{Dr} = 0.75$, V = 13 kV.

including (1) non-welded zone, (2) weld zone, (3) collision zone, and (4) plastic deformation zone (Fig. 4). It was observed from the tensile test results that more weld samples were failed from the plastic deformation zone because the Al sheet was highly stretched in this region, which favors the possibility of necking. Hence, the microstructure evolution of the Al sheet is observed in this zone to investigate the effect of parameters on the tensile properties. Figure 5 indicates the microstructure evolution of Al base metal at different values of sheet thickness.

It was seen from Fig. 5 that an increase in t_{Al} from 0.5 mm (Fig. 5a) to 0.75 mm (Fig. 5b) decreased the grain size of the Al sheet from 34 to 15 µm due to the increase of strain hardening rate. The high value of strain hardening rate is attributable to the increase of impact velocity. On the other hand, the improvement of UTS and degradation of El caused by the increase of t_{Al} from 0.5 to 0.75 mm are owing to the decrease of grain size of the Al sheet around the weld interface. Consequently, the increase of impact velocity of the sheets is responsible for the improvement of UTS and degradation of El. From Fig. 5, an increase in t_{Cu} from 0.3 mm (Fig. 5a) to 0.5 mm (Fig. 5c) was also followed by the decrease of grain size from 34 to 14 µm. The decrease of Al grain size arising from the high impact velocity of the sheets led to an enhancement in the UTS and a reduction in the El. The refinement of Al microstructure from 34 to 9 µm was also observed in Fig. 5 as the value of t_{Dr} elevated from 0.5 mm (Fig. 5a) to 0.75 mm (Fig. 5d). The refinement of Al microstructure in Fig. 5d is more considerable than those observed in Figs. 5b,c, indicating the strong influence of t_{Dr} on the UTS and El.

The influence of sheet thickness on interfacial morphologies of joints was shown in Fig. 6. As can be seen from Fig. 6, the increase of t_{Al} from 0.5 to 0.75 mm changed the morphology of the weld interface from a flat shape (Fig. 6a) to a wavy shape (Fig. 6b) because of the increase of impact velocity. According to Fig. 6c, the increase of t_{Dr} up to 0.75 mm was associated with the nucleation of intermetallic layers and the initiation of vortex formation along the weld interface. The intermetallic layer is generated by partial melting and then rapid solidification of the sheet metals. The vortex mechanism is formed by excessive shearing at the weld interface during the high-velocity impact [3]. Figure 6d shows the simultaneous increase of t_{Al} and t_{Dr} from 0.5 to 0.75, which resulted in the formation of thick intermetallic layers and the completion of vortex formation. To observe the variation of interfacial morphology at the higher impact velocities, the discharge voltage (V) of the EMW device was elevated. The nucleation of a crack along the weld interface was observed in Fig. 6e due to the higher impact velocity of the sheets. Finally, the failure was occurred at the weld interface due to severe collision of the sheets (Fig. 6f). Therefore, by increasing the impact velocity, the following variations would be expected in the interfacial morphology of Al-Cu sheets: (1) change of the morphology of interface from straight to wavy shape, (2) formation of intermetallic layers, (3) formation of

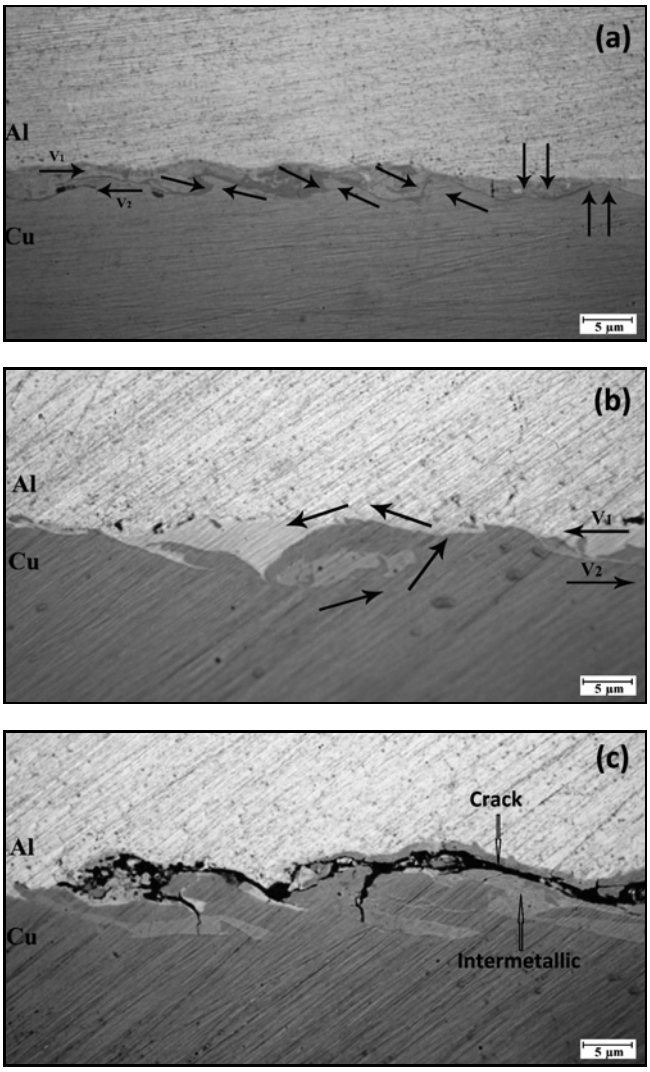

Fig. 7. Formation of (a) wave, (b) vortex, and (c) crack at the weld interface.

vortex, (4) rise of the thickness of intermetallic layers, (5) nucleation of a crack along the interface, and (6) failure of the weld.

Figure 7 indicates the formation of wave mechanism, vortex mechanism, and crack at the weld interface. According to Fig. 7a, when Al and Cu sheets collided together with different velocities, instabilities occurred at the interface due to the interferences. Formation of instability caused material movement from Al side to Cu side, and immediately a material movement from the Cu side to Al side. The newly created interface wave obtained its directionality and shape under the influence of the mutual velocity of the metals. It should be noted that the welded metals have been considered as viscous solids at high impact velocity [13]. A wavy interface increases the strength of the joint due to the strong mechanical interlocking and higher contact area. According to Fig. 7b, along with the progressive collision, a relative tangential velocity at the interface developed, and thus it induced swirling kinematics of the materials at the interface. The materials at the interface twisted and rolled to form a vortex like in a fluidic interface which can be due to a shearing across the interface of two materials. The formation of the vortex also improved the joint strength due to the strong mechanical interlocking [3]. From Fig. 7c, at the high impact velocity of the sheets, the crack was formed at the thick intermetallic layer and propagated along the weld interface, owing to the brittle and fragile nature of the intermetallic layer. The crack formation along the interface reduced the weld width and thus decreased the strength of the joint. Therefore, although the increase of impact velocity results in an increase in the strength of joint due to the formation of wave and vortex phenomena, the intense increase of impact velocity leads to a reduction in the strength of joint due to the formation of the thick intermetallic layers and crack along the weld interface.

To find the chemical composition of the intermetallic layers, SEM-EDX and XRD analyses were performed, Fig. 8. The presence of micro-cracks inside the intermetallic was shown by the SEM image. EDX analysis showed that the intermetallic layer is a combination of Al, Cu, and O elements. However, the atomic percentage of the Al element is more than that of Cu and O elements due to its lower melting temperature. From the XRD analysis in Fig. 8, it can be seen that the compound of $CuAl_2$ was formed within the weld interface of Al-Cu. The formation of the intermetallic phase of $CuAl_2$ can be explained by the nature of the EMSW process. During the EMSW process, the interface of Al-Cu sheets undergoes not only high strain rates but also instantaneous high temperature and high pressure. The high temperature and pressure of the process at the weld interface improved the diffusion of Cu to Al element, which resulted in the formation of the $CuAl_2$ compound.

Figure 9 indicates the microstructure evolution of the sheets around the weld interface. As shown in Fig. 9b, an increase in the values of t_{Al}, t_{Cu}, and t_{Dr} resulted in more plastic deformation of microstructure around the weld interface because of the higher impact velocity of the sheets. Severe plastic deformation of the microstructure near the weld interface is responsible for improving Hv at high values of the thickness parameters.

4.4. Simultaneous improvement of the responses

The desirability function approach was used to optimize the regression models estimated by response surface methodology. Desirability function methodology converted the estimated models (y) to individual

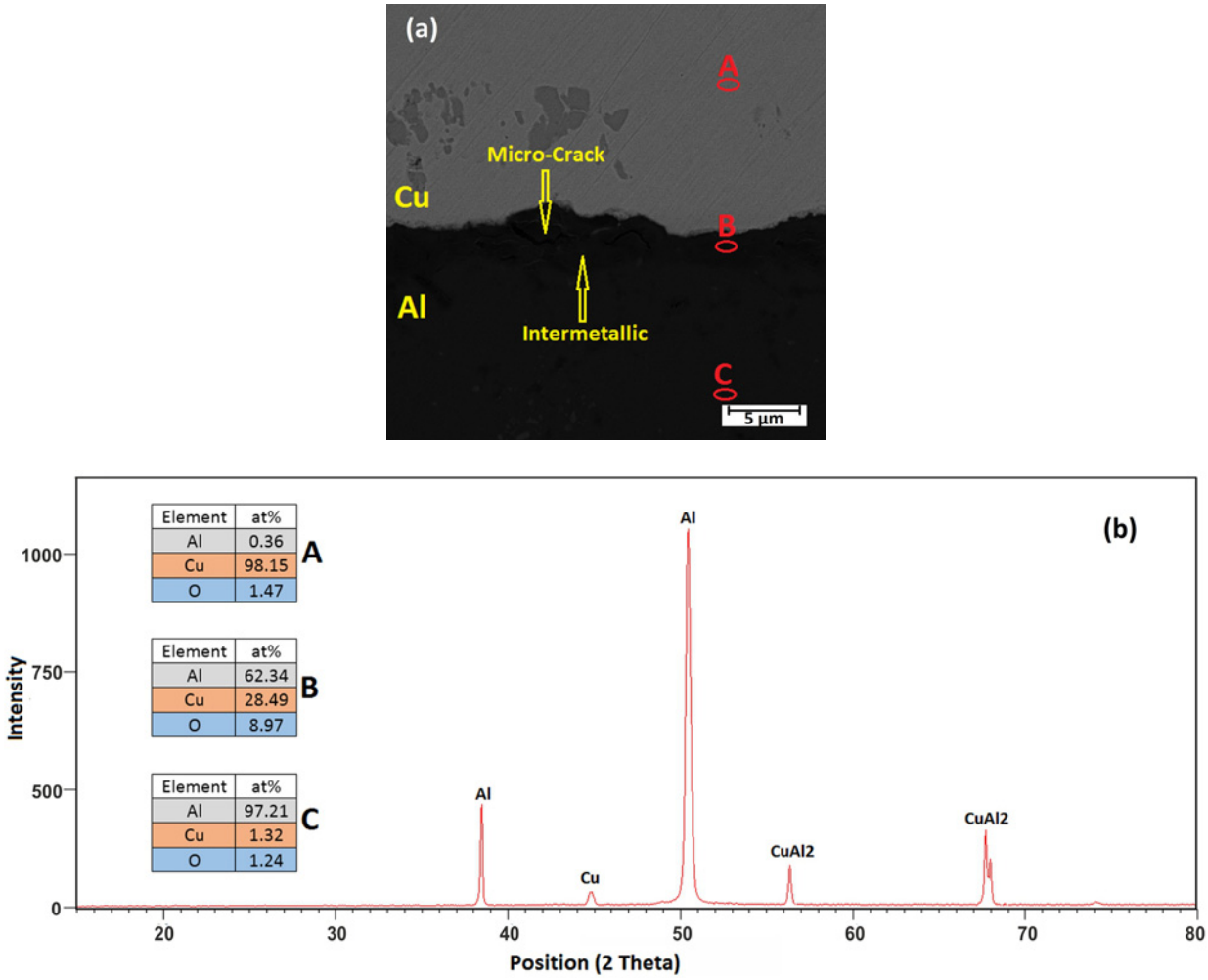

Fig. 8. (a) SEM-EDX and (b) XRD analyses for finding the chemical composition of intermetallic layers.

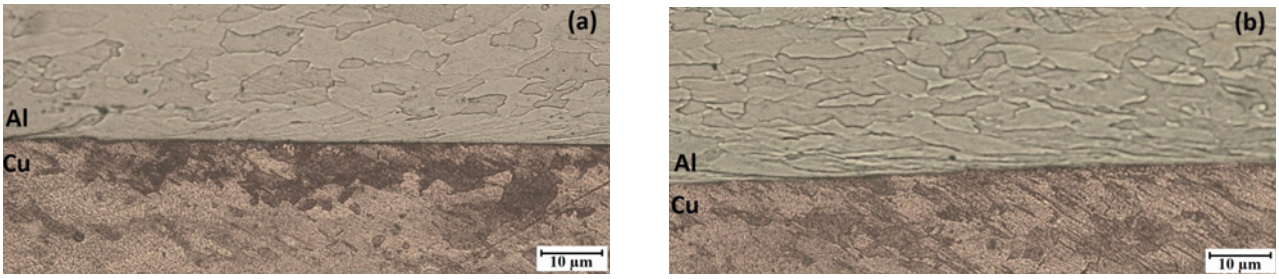

Fig. 9. Microstructure of weld interface observed at parameters of: (a) $t_{\mathrm{Al}} = 0.5$, $t_{\mathrm{Cu}} = 0.3$, $t_{\mathrm{Dr}} = 0.5$ and (b) $t_{\mathrm{Al}} = 0.75$, $t_{\mathrm{Cu}} = 0.4$, $t_{\mathrm{Dr}} = 0.75$.

desirability functions (d) to eventually combine them into a single composite desirability function (D). Individual desirability function (d) varies over the range of zero to one and can be calculated by the following considerations:

(1) the purpose is to maximize the response;

(2) the purpose is to minimize the response;

(3) the purpose is to achieve a particular value of the response.

Since this study aims to enhance the responses (i.e., UTS, El, Ww, and Hv), the individual desirability function is calculated by the first method. To enhance the responses, the following equation can be used, Eq. (4):

$$\begin{cases} 0 & y < L \\ \left(\dfrac{y-L}{T-L}\right)^r & L \le y \le T, \\ 1 & y > T \end{cases} \tag{8}$$

where L and T show the lower and target values of

Table 4. Comparison of the individual and composite desirability for all experiments

Run	Thickness of the sheets (mm)			Individual desirability, d				Composite desirability, D	
	t_{Al}	t_{Cu}	t_{Dr}	UTS	El	Ww	Hv	D	Rank
1	0.5	0.3	0.75	0.612	0.864	0.285	0.435	0.506	13
2	1	0.3	0.75	0.712	0.901	0.262	0.759	0.598	11
3	0.5	0.5	0.75	0.700	0.603	0.936	0.667	0.717	2
4	1	0.5	0.75	0.838	0.490	0.481	0.675	0.604	10
5	0.5	0.4	0.5	0.163	0.829	0.084	0.047	0.152	15
6	1	0.4	0.5	0.278	0.981	0.358	0.672	0.507	12
7	0.5	0.4	1	0.338	0.571	0.382	0.537	0.446	14
8	1	0.4	1	0.521	0.723	0.556	0.722	0.624	8
9	0.75	0.3	0.5	0.430	0.938	0.575	0.619	0.616	9
10	0.75	0.5	0.5	0.670	0.885	0.757	0.817	0.778	1
11	0.75	0.3	1	0.539	0.847	0.655	0.795	0.697	4
12	0.75	0.5	1	0.791	0.380	0.900	0.898	0.702	3
13	0.75	0.4	0.75	0.988	0.229	0.982	0.976	0.683	5
14	0.75	0.4	0.75	0.988	0.229	0.982	0.976	0.683	6
15	0.75	0.4	0.75	0.988	0.229	0.982	0.976	0.683	7

the response, respectively. In the case of exponent r, several conditions have been proposed, including r equal to 1 that shows the liner desirability function, r greater than 1 that gives more importance for the target value, and r between zero and one that gives negligible importance for the target value.

In a multi-response situation, the ideal case of each desirability function is equal to one. In this case, the composite desirability will also be equal to one. The maximum composite desirability function can be computed as the geometric mean of the individual desirability functions. The desirability function approach used in the present study joined four responses into a composite desirability function and can be calculated by the following Eq. (5):

$$D = \sqrt[4]{d_1(\mathrm{UTS}) \times d_2(\mathrm{El}) \times d_3(\mathrm{Ww}) \times d_4(\mathrm{Hv})}, \quad (9)$$

where D represents the composite desirability function, and d_n is the individual desirability function corresponding to each response. The computations related to the desirability function were executed by Minitab® 17 software. The individual and composite desirability functions were attained for all runs of the experiments to select the best combination of the sheet thickness, as given in Table 4.

The experiment with the maximum composite desirability function (D) shows the best combination of the sheet thickness. It can be observed from Table 4 that experiment number 10 has the maximum composite desirability function, and thus it shows the desired thickness of the sheets. To find the optimal thickness of the sheets, the individual and composite desirability functions were also measured for the other thicknesses of the sheets, and the results were shown in Fig. 10.

As can be observed from Fig. 10, to improve all the responses simultaneously, the optimal values of the sheet thickness were predicted as follows: t_{Al} = 0.86 mm, t_{Cu} = 0.5 mm, and t_{Dr} = 0.66 mm. From Fig. 10, it can be also seen that by applying the desirable values of parameters the following values of responses can be achieved: UTS = 73.70 MPa, El= 13.32 %, Ww = 1140.69 μm, and Hv = 53.05 0.1 kgf.

To verify the results of the desirability function, a confirmation experiment was executed at optimal values of parameters, as given in Table 5. The thickness of the sheets was reached to the predicted values by using the fine grade of sandpaper. Table 5 shows that the results of prediction and confirmation experiments are close together with a reasonable percentage error.

5. Conclusions

The simultaneous improvement of the mechanical properties of Al-Cu sheets was obtained by the prediction of the desirable values of sheet thickness in the EMW process. The results of the simulation accurately predicted the formation of a good weld between Al and Cu sheets. When the thickness of Al and driver sheets was 0.75 mm, the maximum values of UTS, Ww, and Hv were obtained, while the value of El was reduced. In the case of the Cu sheet, the maximum values of UTS, Ww, and Hv were obtained at the thickness of 0.5 mm, while it similarly deteriorated the value of El. For simultaneous improvement of UTS, El, Ww, and Hv, it was predicted that the following desirable thickness of the sheets should be applied: t_{Al} = 0.86 mm, t_{SS} = 0.5 mm, and t_{Dr} = 0.66 mm, as validated by a confirmation experiment. Analysis of the microstructure revealed that the grain refinement of Al microstructure around the weld interface caused

Table 5. Comparison of predicted and experimental results at an optimum thickness of the sheets

Response	Predicted result	Experimental result	Percentage error (%)
UTS (MPa)	73.70	72.1	2.17
El (%)	13.32	14.2	6.19
Ww (μm)	1140.69	1087.4	4.67
Hv (0.1 kgf)	53.05	51.8	2.35

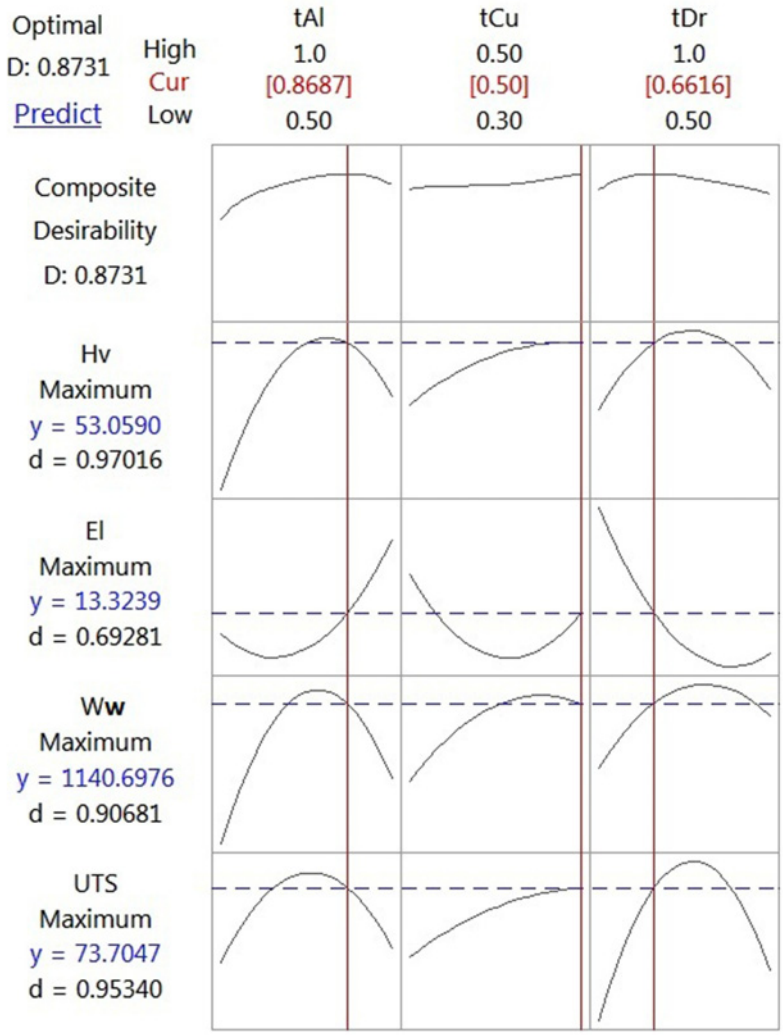

Fig. 10. Simultaneous optimization of the responses by desirability function.

by the higher impact velocity is responsible for the improvement of UTS and deterioration of El. In addition, the main reasons for the improvement of Hv are the deformation of microstructure across the weld interface and the formation of thick intermetallic layers due to the severe collision of the sheets. The increase of impact velocity created the following variations in interface morphology: change of interface from straight to wavy shape, formation of intermetallic, formation of vortex, nucleation of crack, and failure.

References

[1] M. Cheepu, P. Susila, Growth rate of intermetallics in aluminum to copper dissimilar welding, Trans. Indian Inst. Met. 73 (2020) 1509–1514. doi:10.1007/s12666-020-01905-z

[2] R. N. Raoelison, D. Racine, Z. Zhang, N. Buiron, D. Marceau, M. Rachik, Magnetic pulse welding: Interface of Al/Cu joint and investigation of intermetallic formation effect on the weld features, J. Manuf. Process. 16 (2015) 427–434.

doi:10.1016/j.jmapro.2014.05.002
[3] J. S. Li, R. N. Raoelison, T. Sapanathanc, Y. L. Houd, M. Rachik, Interface evolution during magnetic pulse welding under extremely high strain rate collision: mechanisms, thermomechanical kinetics and consequences, Acta Mater. 195 (2020) 404–415. doi:10.1016/j.actamat.2020.05.028
[4] M. Ayaz, M. Khandaei, Y. Vahidshad, Evaluating the electromagnetic welding parameters for improving the mechanical properties of Al-Cu joint, Arab. J. Sci. Eng. 45 (2020) 9619–9637. doi:10.1007/s13369-020-04868-x
[5] C. Li, Y. Zhou, X. Wang, X. Shi, Z. Liao, J. Du, C. Yao, Influence of discharge current frequency on electromagnetic pulse welding, J. Manuf. Process. 57 (2020) 509–518. doi:10.1016/j.jmapro.2020.06.038
[6] M. Pourabbas, A. Abdollah-Zadeh, M. Sarvari, F. Movassagh Alanagh, M. Pouranvari, Role of collision angle during dissimilar Al/Cu magnetic pulse welding, Sci. Technol. Weld. Join. 16 (2020) 549–555. doi:10.1080/13621718.2020.1768351
[7] O. Emadinia, A. M. Ramalho, I. V. D. Oliveira, G. A. Taber, A. Reis, Influence of surface preparation on the interface of Al-Cu joints produced by magnetic pulse welding, Metals 10 (2020) 997–1009. doi:10.3390/met10080997
[8] P. Q. Wang, D. L. Chen, Y. Ran, Y. Q. Yan, X. W. She, H. Peng, X. Q. Jiang, Electromagnetic pulse welding of Al/Cu dissimilar materials: Microstructure and tensile properties, Mater. Sci. Eng. A 792 (2020) 139842. doi:10.1016/j.msea.2020.139842
[9] M. Sarvari, A. Abdollah-Zadeh, H. Naffakh-Moosavy, A. Rahimi, H. Parsaeyan, Investigation of collision surfaces and weld interface in magnetic pulse welding of dissimilar Al/Cu sheets, J. Manuf. Process. 45 (2019) 356–367. doi:10.1016/j.jmapro.2019.07.012
[10] S. A. A. Akbari Mousavi, P. Farhadi Sartangi, Experimental investigation of explosive welding of cp-titanium/AISI 304 stainless steel, Mater. Des. 30 (2009) 459–468. doi:10.1016/j.matdes.2008.06.016
[11] R. N. Raoelison, N. Buiron, M. Rachik, D. Haye, G. Franz, M. Habak, Study of the elaboration of a practical weldability window in magnetic pulse welding, J. Mater. Process. Technol. 213 (2013) 1348–1354. doi:10.1016/j.jmatprotec.2013.03.004
[12] D. C. Montgomery, Design and Analysis of Experiments. John Wiley & Sons, USA, 2005.
[13] A. Ben-Artzy, A. Stern, N. Frage, V. Shribman, O. Sadot, Wave formation mechanism in magnetic pulse welding, Int. J. Imp. Eng. 37 (2010) 397–404. doi:10.1016/j.ijimpeng.2009.07.008